Isolation of Microstructure in Proton-Irradiated Steels

Topical Report
NERI Project 99-0101

A Novel Approach to Materials Development for Advanced Reactor Systems

G. S. Was, M. Atzmon, L. Wang
University of Michigan

September, 2000

DISCLAIMER

INTRODUCTION

Component degradation by irradiation is a primary concern in both current reactor systems as well as advanced designs and concepts where the demand for higher efficiency and performance will be considerably greater. In advanced reactor systems, core components will be expected to operate under increasingly hostile (temperature, pressure, radiation flux, dose, etc.) conditions. The current strategy for assessing radiation effects for the development of new materials is impractical in that the costs and time required to conduct reactor irradiations are becoming increasingly prohibitive, and the facilities for conducting these irradiations are becoming increasingly scarce. The next generation reactor designs will require more extreme conditions (temperature, flux, fluence), yet the capability for conducting irradiations for materials development and assessment in the next 20 years is significantly weaker than over the past 20 years. Short of building new test reactors, what is needed now are advanced tools and capabilities for studying radiation damage in materials that can keep pace with design development requirements.

The most successful of these irradiation tools has been high energy (several MeV) proton irradiation. Proton irradiation to several tens of dpa can be conducted in short amounts of time (weeks), with relatively inexpensive accelerators, and result in negligible residual radioactivity. All of these factors combine to provide a radiation damage assessment tool that reduces the time and cost to develop and assess reactor materials by factors of 10-100. What remains to be accomplished, is the application of this tool to specific materials problems and the extension of the technique to a wider range of problems in preparation for advanced reactor materials development and assessment.

In this project, we plan to approach the mechanism of irradiation assisted stress corrosion cracking (IASCC) by isolating the irradiated microstructure. This report focuses on the microstructure of proton irradiated stainless steel and model alloys for reactor pressure vessel (RPV) steels.

APPROACH

We propose to identify the "persistent" effect responsible for IASCC by separating the

microstructure changes from the microchemistry changes. That is, we propose to create a microstructure typical of that resulting from neutron irradiation in reactor to several dpa, but with *little change* in microchemistry from the unirradiated state. Similarly, we propose to create a microchemistry typical of that resulting from neutron irradiation in-reactor to several dpa, but with *little change* in microstructure from the unirradiated state. In this way, we can perform SCC tests to isolate the key material condition that is responsible for the observed cracking. We do not expect to completely eliminate one feature while completely retaining the other, but we do expect that the feature of interest will strongly dominate the other. We will then be able to conduct more specific investigations into the mechanism by which microstructure or microchemistry changes affect the IG cracking process.

The end result of this program will be the identification of the material changes that affect IASCC and a better understanding of the mechanism. Until such changes are identified, no further progress can be made on identifying the mechanism and solving the problem. Solving the IASCC problem is a long-term goal, but not the objective of this proposal. An understanding of the mechanism will allow for the development of mitigation strategies for existing core components and also the development of radiation-resistant alloys or microstructures for replacement components and for advanced reactor designs. These developments are essential to the extension of existing plants to longer lives and the prevention of IASCC in advanced reactor designs.

The plan of work is based on isolating the relevant LWR microstructure. Experiments will be conducted primarily on commercial purity 304 SS and 316 SS alloys. The alloys will be cold-worked and annealed to produce a grain size of 10-12 micrometers. The commercial alloys were irradiated in reactor and were shown to be susceptible to IASCC via constant extension rate tensile tests. [1] An extensive characterization of their microstructure and microchemistry has been conducted by PNNL and we have shown that both can be replicated by proton irradiation. [2-6] Hence, these alloys represent the ideal case for studying microstructure effects using proton irradiation. Irradiation will be conducted using 3.2 MeV protons generated in the tandetron accelerator at the Michigan Ion Beam Laboratory at the University of Michigan. This produces a nearly flat damage profile over the first 35 μm, followed by a damage peak at ~40 μm. [7] Characterization of microstructure and microchemistry changes will be made in the flat

damage region, away from the surface and the damage peak. Microstructure characterization will be made in TEM and microchemistry characterization will be made using STEM-EDS. The effect of microstructure will be evaluated for IASCC susceptibility using CERT tests. We will focus IASCC experiments on the 304 SS alloy because of its greater propensity for IASCC. This report covers microstructure formation and characterization.

EXPERIMENT

Alloys of 304 SS and 316 SS were selected for microstructure study following proton irradiation at 360°C over a range of doses and in different initial conditions. Model RPV alloys were selected to isolate the effects of Cu and Mn on the hardness and microstructure following proton irradiation at 300°C over a range of doses. The chemical compositions for all the alloys used in this study are listed in table 1, and a summary of irradiation conditions for each alloy used in this work is listed in table 2.

All alloys were used in the as-received condition, in the form of bar samples made by electric discharge machining (EDM) to minimize the mechanically damaged layer. No heat treatment was given to these samples. After wet polishing, all stainless steel samples were electropolished in a solution of 60% phosphoric acid and 40% sulfuric acid for 3 min at approximately 42°C to provide a smooth surface prior to irradiation. Model RPV alloys were electropolished in a solution of 65% methanol, 28% nitric acid and 7% 2-butoxyethanol.

Sample irradiations were performed using a tandem accelerator (the General Ionex Tandetron) at the Michigan Ion Beam Laboratory for Surface Modification and Analysis at the University of Michigan. All irradiations were conducted using 3.2 MeV protons in a vacuum better than 3×10^{-8} torr. Protons with this energy produce a nearly uniform damage layer in the first 35 μm of the proton range (40 μm) as calculated using TRIM97. [8] Stainless steel samples were irradiated at 360°C to between 0.1 and 5.0 dpa. Model RPV alloys were irradiated at 300°C to doses between 0.001 and 0.01 dpa. The dose uniformity of the irradiated stainless steel samples was checked using a Tennelec LB 5100 automated alpha/beta counter by measuring the activity in units of β-counts/min/mm^2 for each sample within the same irradiation batch.

Irradiated bar samples were back thinned to a thickness of ~300 μm from the unirradiated side using wet polishing (180-320 grit SiC paper). TEM disks were cut using a slurry drill core-cutter to minimize mechanical damage. TEM disks were further wet-polished from the unirradiated side down to a thickness of 100~140 μm using 400-2400 grit SiC paper. After removing ~5 μm from the irradiated side, samples were jet-polished from the unirradiated side until perforation occurred.

Microstructure analysis on stainless steel alloys was carried out using transmission electron microscopy on a JEOL® 2000FX TEM/STEM. Bright field (BF) imaging, dark field (DF) imaging and rel-rod dark field (RRDF) imaging techniques were used to characterize the microstructure before and after proton irradiation. A minimum of four TEM images (at magnification=100K to 200K) were taken for each condition in order to obtain a reliable measure of loop density and size. Model RPV alloy microstructures were analyzed in the JEOL 2010F. Both bright field and dark field techniques were used to characterize the precipitate character of the sample. Small angle x-ray scattering (SAXS) was also used to evaluate the precipitate structure of the irradiated model alloys. Anomalous small angle x-ray scattering was conducted on the SAXS beam line at the Advanced Photon Source (APS) at a photon energy of 7.09 keV, with the help of Dale Alexander of Argonne National Laboratory.

To evaluate radiation induced hardening, yield strength changes were estimated from Vickers hardness measurements before and after irradiation. At least 20 measurements were made using a 25g load at room temperature. According to Higgy and Hammad [9] the yield strength changes due to irradiation for 304 SS can be estimated from hardness changes using the relation:

$$\Delta\sigma_y = 3.54\,\Delta H_y \quad , \qquad (1)$$

where ΔH_V is in kg/mm^2 and $\Delta\sigma_y$ is in MPa. For the Fe-base model RPV alloys, the conversion factor is 3.62. [10] If the unirradiated yield strength is known, the yield strength for the irradiated material can be determined.

Radiation-induced hardening in the stainless steels was also determined from microstructure measurements by calculating the yield strength change using the dispersed-barrier-hardening model [11] for dislocation loops:

$$\Delta\sigma_y = 3.06\alpha\mu b\sqrt{Nd} \quad , \quad (2)$$

where α is the barrier strength factor (1.0 for voids and 0.4 for faulted loops), μ is the shear modulus, b is the Burgers vector for network dislocation, N is the defect number density, and d is the mean size of the defects. For austenitic stainless steels, $\mu \approx 76$ GPa and $b=2.55\times10^{-8}$ cm were used for calculation.

RESULTS AND DISCUSSION

The results for the proton-irradiated microstructure and irradiation-induced hardening (yield strength increase) as a function of irradiation dose at fixed temperature are presented in comparison with the neutron-irradiated microstructures. Results on dislocation loop characterization are presented first, followed by irradiation hardening. Results on stainless steel are presented first, followed by those on model RPV alloys.

Stainless Steels

Microstructure Characterization

TEM examination indicated that dislocation loops are the dominant irradiation-induced microstructure feature for all the proton irradiation conditions investigated. Figure 1 shows rel-rod dark field images of the Frank loops as a function of irradiation dose for CP 304 SS and CP 316 SS. Loop size distributions measured from proton- and neutron-irradiated commercial purity CP 304 SS and CP 316 SS are shown in Fig. 2. At comparable doses, loop size distributions for neutron irradiation at 275°C and proton irradiation at 360°C are in good agreement. This confirms that loop structure development under neutron irradiation (275°C, 7×10^{-8} dpa/s) and proton irradiation (360°C, 7×10^{-6} dpa/s) is basically the same despite the difference in displacement morphology due to differences in particle type.

Loop densities resulting from proton irradiations are plotted together with those from neutron irradiation as a function of dose in Fig. 3. Note that the alloys used for neutron irradiation at 275°C and for proton irradiation at 360°C are from the same heat, providing direct comparison of microstructure evolution between neutron and proton irradiation without concern for the difference in composition and heat treatment. Loop densities in proton-irradiated CP 304

SS and CP 316 SS follow the same trend as for neutron irradiation at 275°C. This indicates that the partitioning of point defects to loops and other sinks, the balance between nucleation and loss of loops by loop unfaulting and interstitial cluster diffusion, and the evolution of overall sink strength are similar for neutron and proton irradiation. While the trends are in good agreement, the loop density in proton-irradiated CP 304 SS at 360°C is slightly lower than that for neutron irradiation at 275°C. It appears that the difference in loop densities between neutron and proton irradiation diminishes with increased dose. One of the possible reasons for the larger difference at low dose may be the greater difficulty in imaging small loops at low doses where the size is small. The JEOL 2000F used at Michigan for characterization of proton-irradiated microstructures does not have the same imaging capability as the JEOL 2010F used at PNNL for characterizing the neutron-irradiated microstructures used for comparison.

The dose dependence of loop size for proton-irradiated CP 304 SS and CP 316 SS, and high purity alloys is shown in Fig. 4, together with neutron data (275°C, 300°C and 390°C) taken from references [12-16] The data for proton- and neutron-irradiated CP 304 SS and CP 316 SS taken from the same heat are in good agreement. The magnitude of the loop size for proton-irradiated CP 304 SS and CP 316 SS is consistent with that of neutron irradiation. Loop size rapidly increases with dose at doses below 1 dpa, approaching saturation between 3 and 5 dpa.

Proton irradiation can achieve damage rates several orders of magnitude higher than that of neutron irradiation in LWR core components. To maintain an equal fraction of defect loss to recombination as for neutron irradiation, and to have the same defect partitioning to the microstructure, an elevated temperature is required. However, the effect of elevated temperature on the overall sink strength could also influence the microstructure development. For example, the annihilation of network dislocations is promoted and the loop loss by small interstitial cluster diffusion to sinks is also increased by the upward temperature shift.

The microstructures resulting from neutron and proton irradiation can still be very similar if the effects of higher dose rate, higher temperature and smaller cascades for proton irradiation on the defect partitioning and sink development are balanced. Therefore, the physical process for a rapid increase in loop density and size at low dose and the tendency to saturation for loop density and size at higher dose should be the same for both neutron and proton irradiation. Results show that the magnitude of faulted loop density and size at saturation from proton

irradiation can be controlled to be very close, if not the same, to that of neutron irradiation by adjusting the proton irradiation temperature at a given dose rate.

Irradiation-Induced Hardening

The dose dependence of hardening in proton-irradiated austenitic alloys is shown in Fig. 5. Hardening from proton irradiation was determined from Vickers hardness data and that from neutron irradiation was determined via the shear punch technique. For comparison, hardness increases using both techniques were converted to yield strength increases in units of MPa. Note that the agreement between neutron- and proton-irradiation induced hardening is excellent across the entire dose range.

Figure 6 shows a comparison between measured (Vickers or shear punch) hardness and hardness calculated from the dislocation loop microstructure using eqn. (2). Results are in fairly good agreement across the hardness range (larger hardness occurs at higher dose), especially for proton irradiation. The only anomaly is the higher dose neutron-irradiated results for the 304 SS samples, where the hardness determined from microstructure exceeds that measured from the irradiated sample.

The comparison between proton and neutron results on these two heats and the existing database is shown in Fig. 7. The dose dependence of yield strength evaluated from hardness and microstructure measurements for proton-irradiated commercial purity alloys is compared with neutron data [17-20]. An unirradiated yield strength value of 243 MPa for CP 304 SS and 228 MPa for CP 316 SS was added to the irradiation-induced yield strength change to obtain the irradiated yield strength. To increase the clarity, two lines were drawn to mark the boundaries of the neutron data, Fig. 7 (a), then the neutron data were removed and proton data were superimposed on the boundaries for comparison, Fig. 7 (b). The proton data are within the neutron data band except for the two data points for CP 304 SS at 3 dpa. That the proton data fall within the neutron data band is expected since the irradiation condition was designed to generated equivalent microstructure for LWR conditions around 300°C. The close agreement with neutron data justified the use of proton irradiation to produce the same amount of irradiation hardening as does neutron irradiation.

Model RPV Alloys

Microstructure Characterization

The bulk of the characterization of the microstructure of the model alloys is by SAXS, with only preliminary data from TEM. In these experiments, the VD alloy was irradiated to two doses and subsequently analyzed by SAXS. Measurement was taken at an energy of 7.090 keV. The relation between q and I is shown in Fig 8. From this figure, samples at both dose levels, 0.01 dpa and 0.001 dpa, produced higher scattering intensity than the unirradiated ones. The 0.01 dpa dose sample has stronger intensity than 0.001 dpa sample, indicating a higher density or larger size scattering centers. The intensity of the 0.01 dpa dose sample drops as q increases, approaching the curve for the unirradiated sample at high q values and angles. With the angle of X-ray scattering increasing, the upper limit of the structure size, which the scattering can reflect, will decrease. At large angles, X-ray scattering is not sensitive to larger structures. At the corresponding (low) size, the scattering is no different between an irradiated and an unirradiated sample, so the signals overlap. It should be noted that the curve for the 0.001 dpa sample does not approach that for the unirradiated sample at high q. This is likely due to contamination from Kapton tape used in the experiment. Kapton tape is used to suspend the foil samples in the X-ray beam. Unfortunately, our current set up resulted in slippage of a stepper motor, resulting in mis-positioning of the sample in the beam. In the low dose proton case, some of the kapton tape was intercepted and scattering from it was superimposed upon the sample signal.

The relation between ln$I$ (where I represents the difference between the irradiated and the unirradiated signals) and q^2 is shown as Fig. 9. From Guinier's approximation [21] we obtain:

$$I(q) = I_0 \exp\left(-\frac{q^2 R_G^2}{3}\right) \tag{3}$$

where $\vec{q}$ is the scattering vector which defines the geometry of the experiment. For small angles, 2θ, the modulus q is $2\pi\theta/\lambda$. R_G is particle radius of gyration. Equation (4) can be rewritten as:

$$\ln I(q) = K - \frac{R_G^2}{3} q^2 \tag{4}$$

From the slope of a plot of $lnI(q)$ *vs.* q^2, we obtain directly, the radius of gyration, R_G and then the particle radius, $R=(5/3)^{1/2}R_G$ (assuming spherical particles). Phythian [22] confirmed the spherical symmetry of the strain field around the precipitates in Fe-1.3Cu model alloy through TEM. For both doses, we obtain excellent linear fits to the data. From eqn. (5), the precipitate radius in the 0.001 dpa dose sample is about 7.1 Å, and in the 0.01 dpa dose sample it is 16.0 Å. The low dose size is smaller than that resulting from electron irradiation [23] 11.8 Å (VD, 0.0005dpa, $7.5x10^{-9}$dpa/s, 300°C). However, the high dose precipitate size is close to that following neutron irradiation to ~0.013dpa (1.8 nm for a 1-feature fit and 1.0 and 2.0 nm for a 2-feature fit). [24] The Guinier approximation is strictly valid in the range $qR_G<<1$ 0. [25] In these measurements, R_G is 5.5Å for the low dose and 12.4Å for the high dose, yielding values of qR_G. in the range 0.5 to 1.2. Therefore, the approximation is not ideal for these measurements. In future work, the maximum entropy method will be applied to the data.

Irradiation-Induced Hardening

Hardening in model RPV alloys can result from two sources, the dislocation microstructure induced by irradiation and second phase particles. Results from hardness measurements following irradiation of alloys VD and VA are given in table 3 and are compared to those from neutron irradiation in Figure 10. The unirradiated hardness values for each alloy represent an average of the values of several different samples. Results for the VD alloy are very encouraging in that both the magnitude of the hardness increase and the trend with dose is very similar to that found after neutron and electron irradiation. The amount of hardening at all dose levels is essentially indistinguishable from that due to neutrons. Of equal interest is the hardening of the VA alloy (Fe only), which is similar to that of the Fe-1.0Mn alloy irradiated with neutrons. The fact that the hardness increase is only about 1/6 that of the Fe-Cu-Mn alloy at the same dose indicates that something other that radiation damage (dislocation hardening) is contributing to the hardening of the Fe-Cu-Mn alloy. Given the magnitude of the hardness increase, the likely cause is precipitation of Cu-rich clusters. Subsequent annealing of the 0.01 dpa VD alloy at 450°C for 24 hrs resulted in a drop in hardness by about 25 MPa, or about 30% of the as-irradiated hardness increase. These values are in good agreement with those of Lucas et al. [26] who found that a 0.35Cu-0.6Ni model alloy experienced 40% recovery of the as-irradiated hardness increase after the same time at temperature. The magnitude of the drop is

further indication that the hardness of the irradiated alloy is likely due to precipitates. The drop in hardness is likely due to precipitate coarsening.

Taken together with the SAXS data on the microstructure, these results are consistent with hardening by a high density of very small precipitates, and the hardening is similar in trend and magnitude to that resulting from neutron irradiation of the same alloys.

SUMMARY

The objective of this work was to understand the microstructure evolution in stainless steel and model alloys of reactor pressure vessel steel under LWR irradiation conditions. This work focused on investigating the irradiated microstructure by using proton irradiation in comparison with neutron irradiation. The following points summarize the results of the study:

1) The irradiation-induced microstructure in proton-irradiated austenitic stainless steels consists mainly of dislocation loops up to 5.0 dpa.

2) The dose dependence of the dislocation loop density and size in proton-irradiated Fe-Cr-Ni alloys follows the same trend as in neutron-irradiated alloys. The higher loop density in commercial alloys is probably due to enhanced nucleation of loops by minor constituent elements (phosphorus, silicon).

3) Yield strength in proton-irradiated austenitic alloys as a function of dose and temperature are consistent with the neutron data trend. Across the entire dose range, the hardening estimated from hardness measurements agrees with calculations based on the dispersed barrier hardening model.

4) Hardening analysis of proton-irradiated model RPValloys show that the amount of hardening is comparable to that from neutron irradiation at the same temperature and to the same dose. Annealing of the irradiated microstructure produces a recovery of hardening that also matches that from neutron irradiation. SAXS data shows that the precipitate size/density combination is similar to that from neutron irradiation.

5) The difference in the effect of the character of the displacement cascade on loop nucleation between neutron irradiation (275°C, 7×10^{-8} dpa/s) and proton irradiation (360°C, 7×10^{-6} dpa/s) has little effect on the final irradiated microstructure. The reduced level of loop

nucleation by in-cascade interstitial clustering in proton irradiation appears to be balanced by the higher cascade efficiency and higher vacancy supersaturation caused by the higher dose-rate and the lower sink strength at the higher irradiation temperature.

REFERENCES

1. H. M. Chung, W. Ruther, J. Sanecki, A. Hins, N. Zaluzec and T. Kassner, *J. Nucl. Mater.* 239 (1996) 61.
2. G. S. Was and T. Allen, JNM 205 (1993) 332.
3. D. L. Damcott, G. S. Was and S. M. Bruemmer, *Proc. Materials Research Society*, Vol. 373, Materials Research Society, Pittsburgh, 1995, p. 131.
4. R. D. Carter, D. L. Damcott, M. Atzmon, G. S. Was and E. L. Kenik, *J. Nucl. Mater.* 205 (1993) 361.
5. R. D. Carter, M. Atzmon, G. S. Was and S. M. Bruemmer, *Proc. Materials Research Society*, Vol. 373, Materials Research Society, Pittsburgh, 1995 p. 171.
6. T. Allen, G. S. Was and E. Kenik, *J. Nucl. Mater.*, 244 (1997) 278.
7. D. Damcott, D. Carter, J. Cookson, J. Martin, M. Atzmon and G. S. Was, *Rad. Eff. Def. Sol.* 118 (1991) 383.
8. J. F. Zigler, J. P. Biersack and U. Littmark, The Stopping and Range of Ions in Solids, Pergamon Press, New York, 1966.
9. H. R. Higgy and F. H. Hammad, J. Nucl. Mater. 55 (1975) 177.
10. J. F. Mancuso, J. A. S;pitznagel, R. P. Shogan and J. R. Holland, in Effects of Radiation on Materials: Tenth Conference, ASTM STP 725. D. Kramer, H. R. Brager and J. S. Perrin, eds., American Society for Testing and Materials, 1981, pp. 38-48.
11. G. E. Lucas, J. Nucl. Mater. 20 (1993) 287-305.
12. S.M. Bruemmer, EPRI report, RP 4068-20, Oct. 1997
13. Oddet & Lucas, DOE-ER 0313/6 (1989)
14. Tanaka et al., J. Nucl. Mater., 179 (1991) 572
15. Maziasz, ORNL-6121 (1985)
16. S.J. Zinkle, P.J. Maziasz and R.E. Stoller, J. Nucl. Mater., 206 (1993) 266-286.
17. G.E. Lucas, J. Nucl. Mater. 206 (1993) 287-305

18. M. Kodama, et al., Proceeding of 8th International Symposium On Environmental Degradation of Materials In Nuclear Power System – Water Reactors, (1998) p. 831

19. Odette and Lucas, DOE/ER-0313/6 (1989)

20. A. Jensen, et al., EPRI report, 1998

21. Guinier, (1938), Nature 142,569

22. Phythian, W. J., Foreman, A. J. E., *et al*, "the Structure and hardening Mechanism of Copper Precipitation in Thermally Aged or Irradiated Fe-Cu and Fe-Cu-Ni Model Alloys," Effects of Radiation on Material:15th International Symposium, ASTM STP 1125, Philadelphia, 1992, pp.131-150.

23. Alexander, D. E., Kestel, B. J., *et al*, "Correlating Radiation Exposure with Embrittlement : Comparative Studies of Electron- and Neutron- Irradiated Pressure Vessel Alloys," ASTM 1398, West Conshohocken, PA, 2000

24. G. R. Odette, unpublished results.

25. Eric Lifshin, X-ray Characterization of Materials, Wiley-VCH,1999, pp.221.

26. G. E. Lucas, E. Mader and G. R. Odette, Proc. 4th Int'l Symp. Environmental Degradation of Materials in Nuclear Power Systems – Water Reactors, National Association of Corrosion Engineers, Houston, TX, 1990, pp. 2-1 to 2-25.

List of Figures

1. Photomicrographs showing dislocation loops in bright field images as a function of irradiation dose at 360°C for a) CP 304 SS and b) CP 316 SS.
2. Comparison of loop size distribution between neutron-irradiated (275°C) and proton-irradiated (360°C) CP 304 SS (a) and CP 316 SS (b).
3. Dose dependence of faulted loop density between neutron-irradiated (open symbols) and proton irradiated (solid symbols) CP 304 and CP 316 stainless steels.
4. Dose dependence of the loop size in neutron-irradiated (open symbols) and proton irradiated (solid symbols) CP 304 and CP 316 stainless steels.
5. Dose dependence of yield strength change calculated from microhardness (proton-irradiated alloys) and both CP 304 SS and CP 316 SS.
6. Yield strength increase as determined from hardness or shear punch measurements and compared to that determined from the microstructure for proton-irradiated and neutron-irradiated CP 304 SS and CP 316 SS.
7. (a) Measured yield strength of 300 series austenitic stainless steels irradiated with neutrons and tested at approximately 300°C, and (b) estimated yield strength increase in proton irradiated CP 304 SS and CP 316 SS plotted against the neutron data trend.
8. The relation between $ln\ I$ and q^2 for the VD alloy following proton irradiation to doses of 0.001 and 0.01 dpa at 300C at a dose rate of 7×10^{-7} dpa/s.
9. Yield strength increase as a function of dose for several alloys and several irradiating particles (n = neutron, p = proton, e = electron).

Table 1. Composition of alloys used in this work (wt%)

Alloy	Fe	Cu	Cr	Ni	Mn	Mo	Si	C	N	P	S
CP 304 SS	Bal.	-	18.3	8.5	1.38	0.37	0.65	0.035	0.068	0.03	0.03
CP 316 SS	Bal.	-	16.7	12.2	1.75	2.58	0.59	0.04	0.058	0.02	0.01
VD	Bal.	0.9	-	-	1.0	-	-	-	-	-	-
VA	Bal.	-	-	-	-	-	-	-	-	-	-

Table 2. Summary of irradiation conditions used in this work

Alloy	Temperature (°C)	Dose (dpa)
CP 304 SS	360	0.5
	360	1.0
	360	3.0
	360	5.0
CP 316 SS	360	1.0
	360	3.0
	360	5.0
VD (Fe-0.9Cu-1.0Mn)	300	0.001
	300	0.003
	300	0.01
VA (Fe)	300	0.001
	300	0.003

Table 3. Hardness and yield strength changes in alloys VA and VD following proton irradiation at 7 x 10^{-7} dpa/s and 300°C.

	VD alloy				VA alloy			
Dose (dpa)	H_v^{irrad} (kg/mm^2)	ΔH (kg/mm^2)	$\Delta\sigma$ (MPa)	$\Delta\sigma_{avg}$ (MPa)	H_v^{irrad} (kg/mm^2)	ΔH (kg/mm^2)	$\Delta\sigma$ (MPa)	$\Delta\sigma_{avg}$ (MPa)
0.001	159.0	53.0	192		92.2	9.7	35.1	
	157.0	51.0	185	189	91.9	9.4	34.0	34.6
0.003	165.2	59.2	216		91.5	9.0	32.6	
	166.7	60.7	220	218	92.2	9.7	35.1	33.9
0.01	184.8	78.8	285					
	190.8	84.8	307	296				
0.01+ 450°C/24 hrs	**176**	**61.0**	**221**	**221**				

H_v° for alloy VD = 107 kg/mm^2, H_v° for alloy VA = 82.5 kg/mm^2

$\Delta\sigma$ (MPa) = 3.62 x ΔH(kg/mm^2)

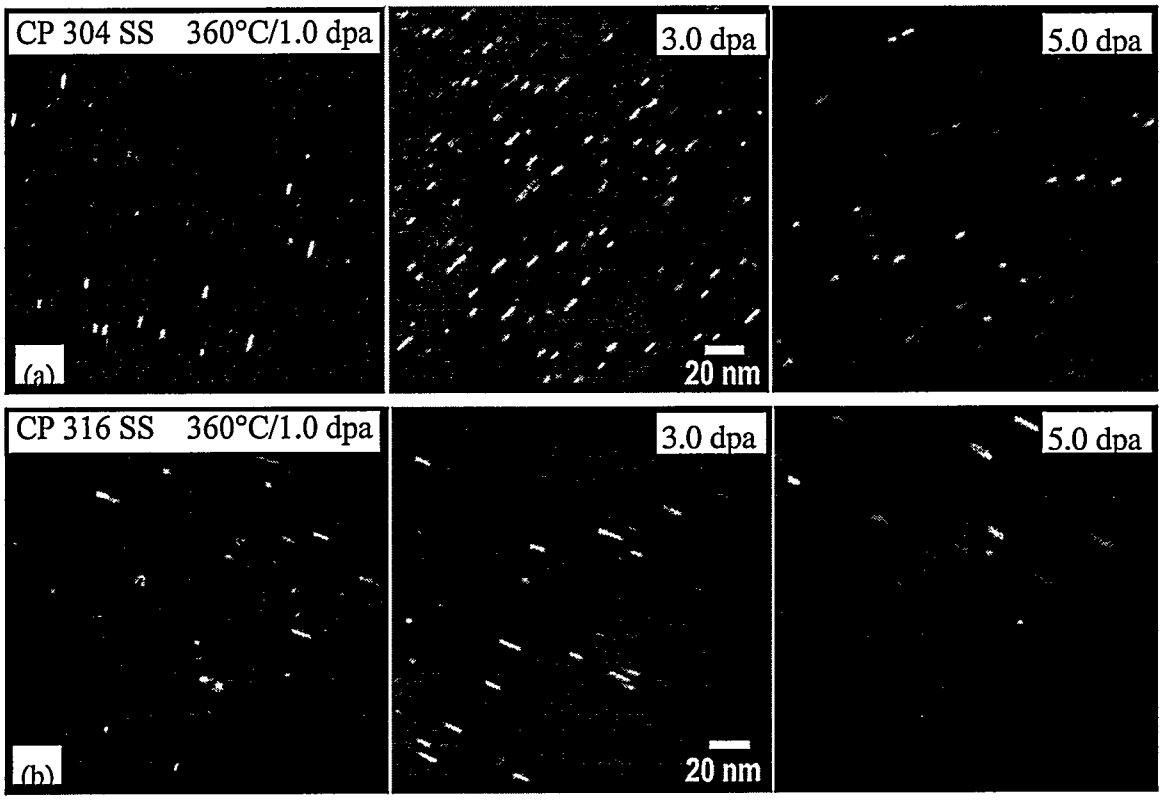

Figure 1. Photomicrographs showing dislocation loops in dark-field images as a function of irradiation dose at 360 °C for a) CP 304 SS and b) CP 316 SS.

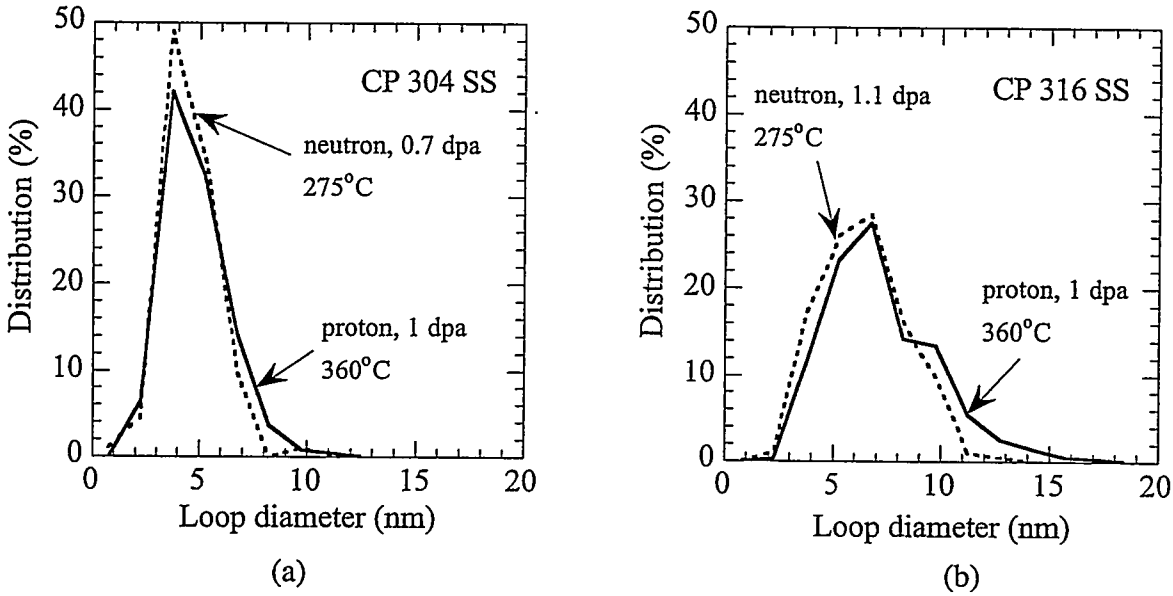

Figure 2. Comparison of loop size distribution between neutron-irradiated (275°C) and proton-irradiated (360°C) CP 304 SS (a) and CP 316 SS (b).

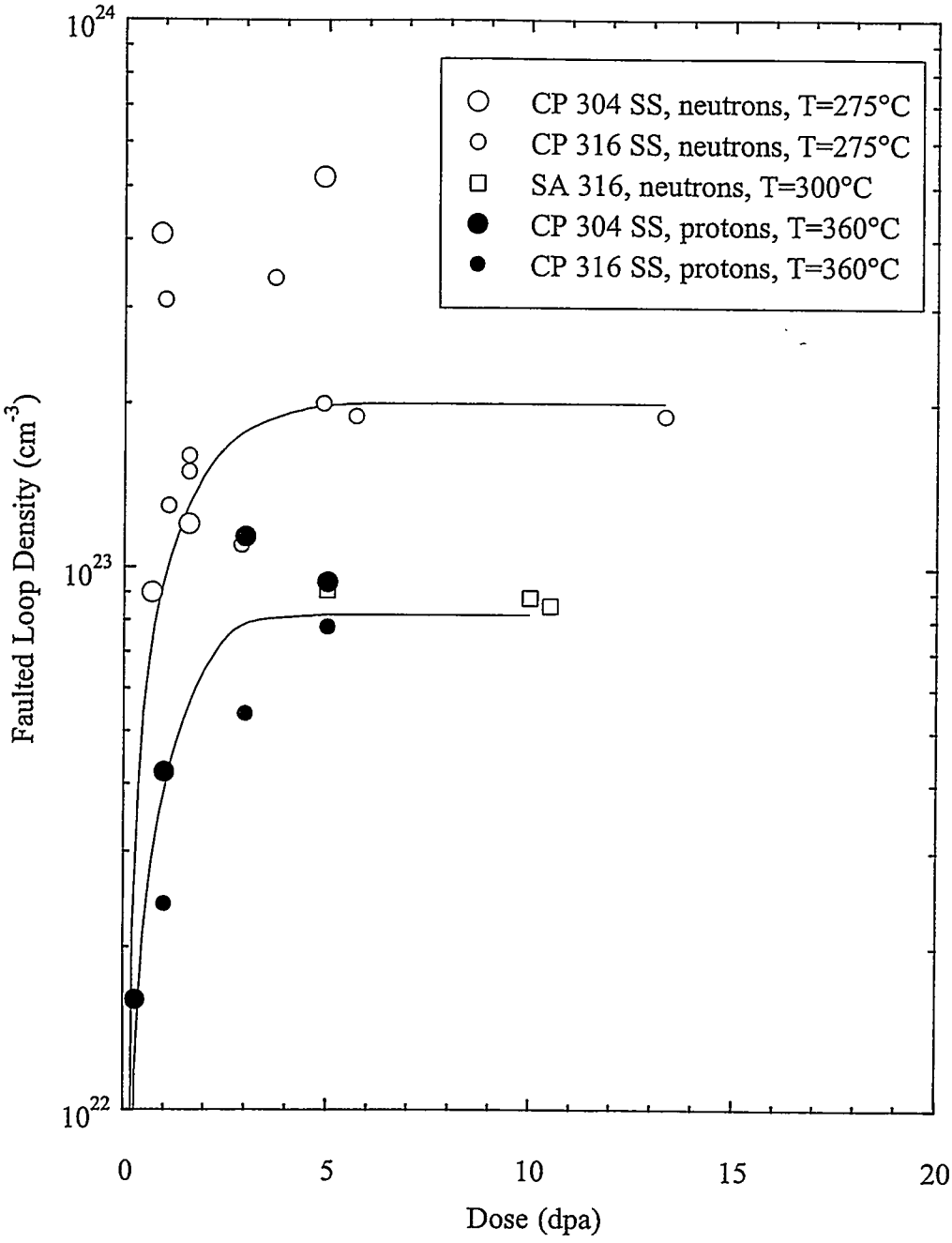

Figure 3. Dose dependence of faulted loop density between neutron-irradiated (open symbols) and proton irradiated (solid symbols) CP 304 and CP 316 stainless steels.

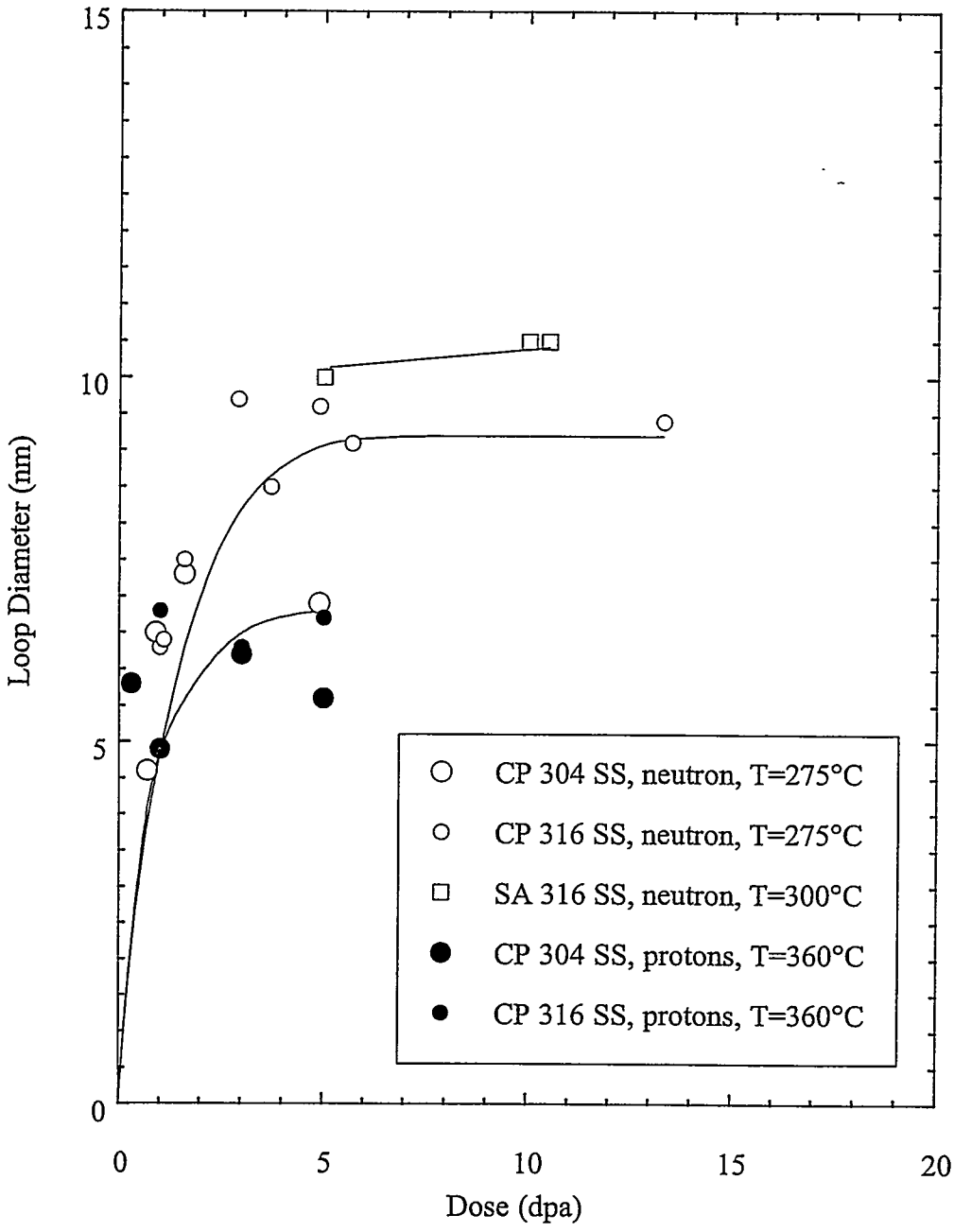

Figure 4. Dose dependence of loop size in neutron-irradiated (open symbols) and proton irradiated (solid symbols) CP 304 and CP 316 stainless steels.

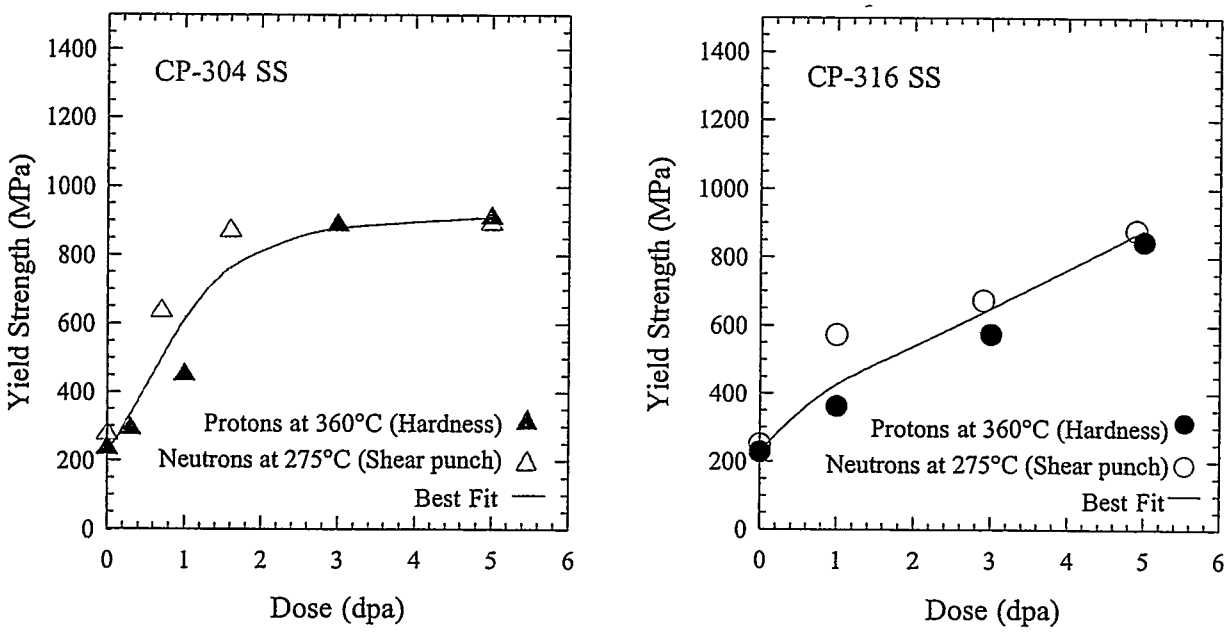

Figure 5. Dose dependence of yield strength change calculated from microhardness (proton-irradiated alloys) and measured by the shear punch method (neutron-irradiated alloys) for both CP 304 SS and CP 316 SS.

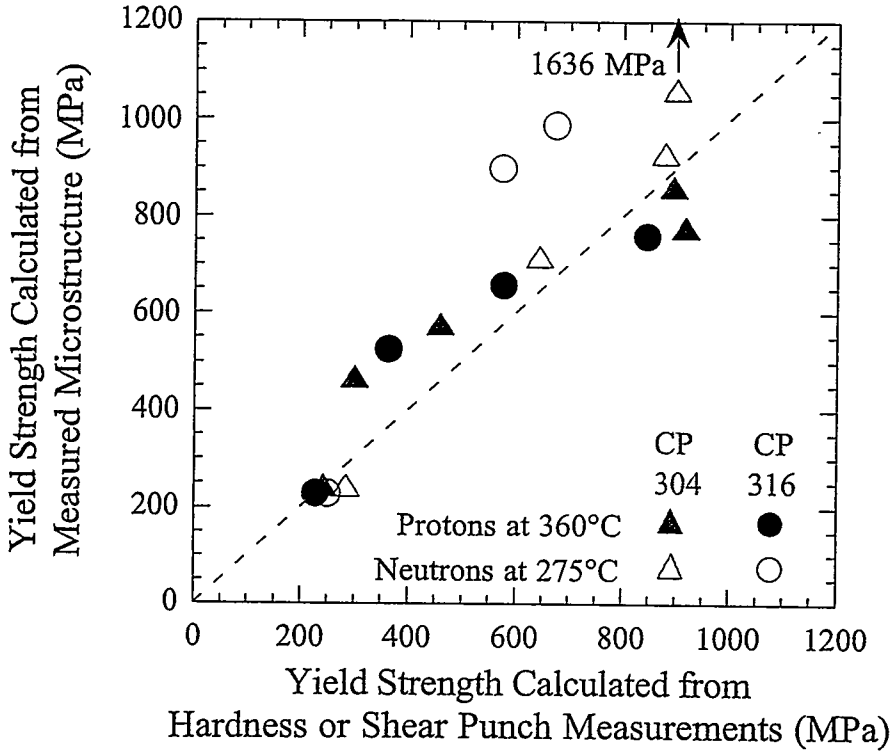

Figure 6. Yield strength increase as determined from hardness or shear punch measurements and compared to that determined from the microstructure for proton-irradiated and neutron-irradiated CP 304 SS and CP 316 SS.

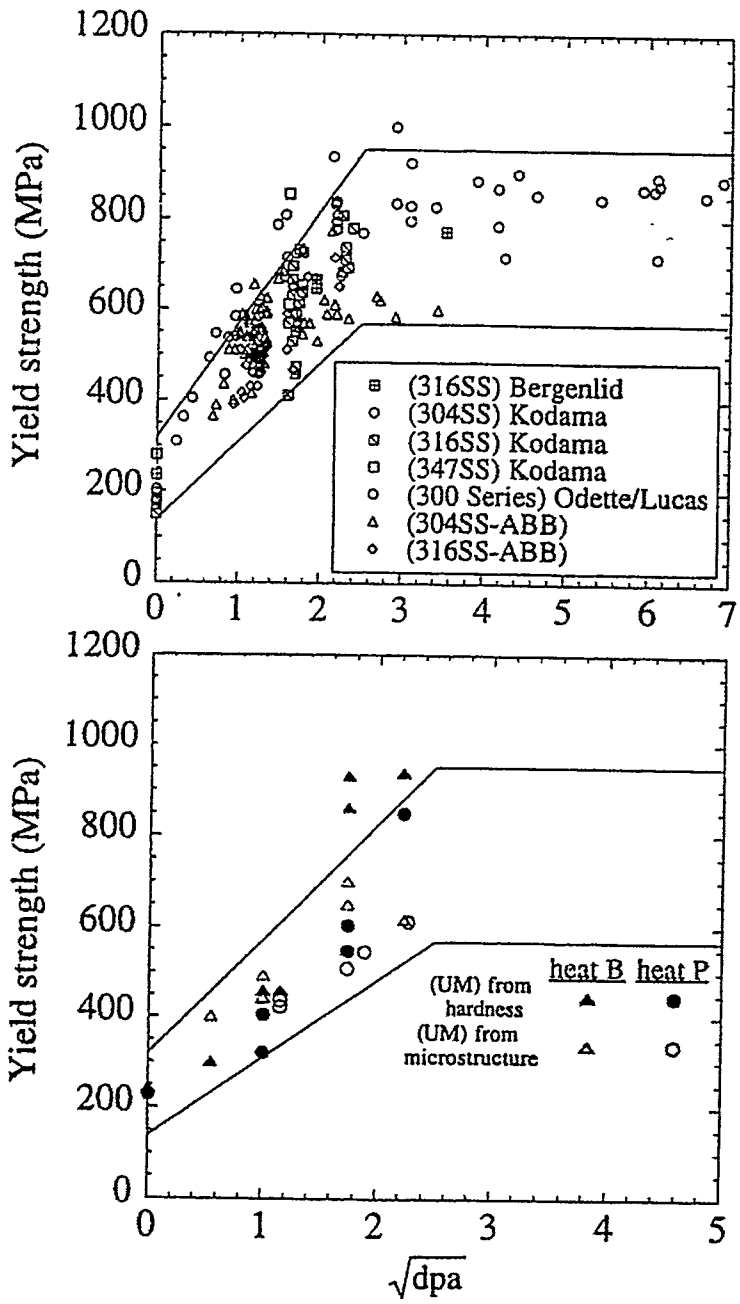

Figure 7. (a) measured yield strength of 300 series austenitic stainless steels irradiated with neutrons and tested at approximately 300°C, and (b) estimated yield strength increase in proton irradiated CP 304 SS and CP 316 SS plotted against the neutron data trend.

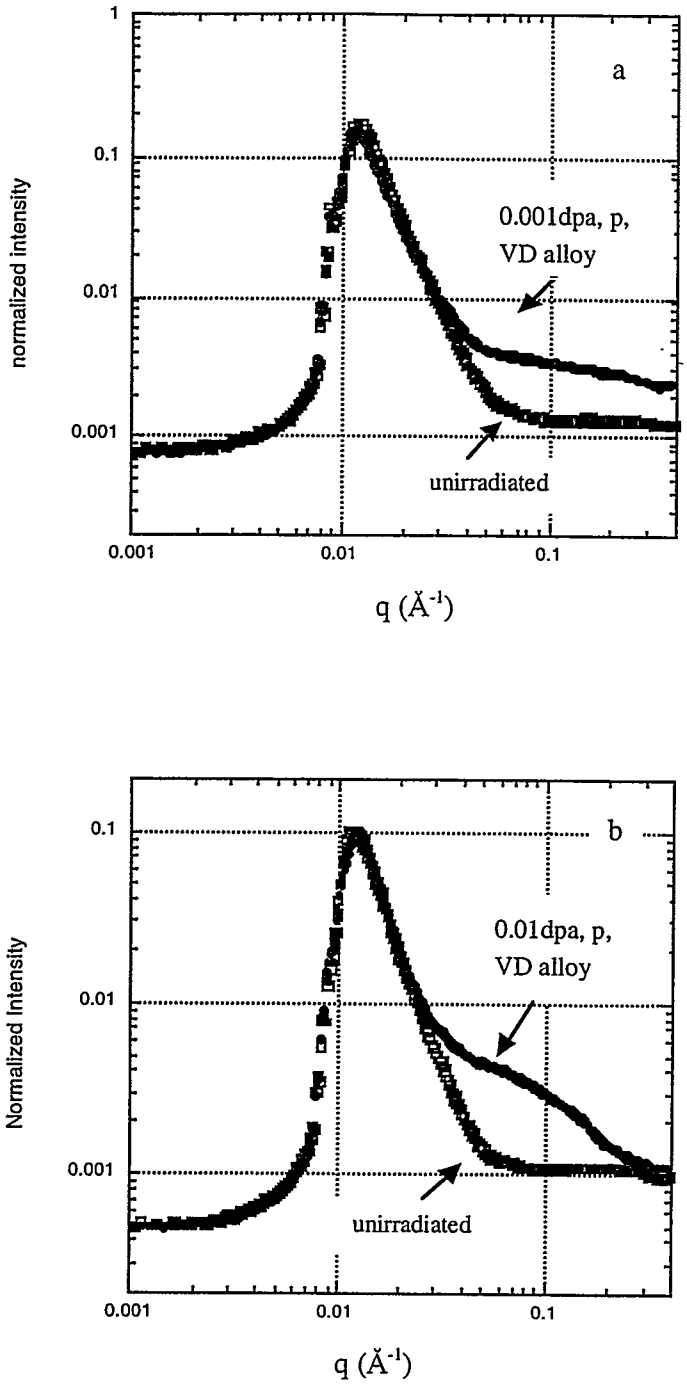

Figure 8. The relation between scattering vector q and X-ray (E=7.090*ke*V) intensity I for a)0.001 dpa and b)0.01 dpa proton (3.2MeV) irradiation at 300°C for VD alloy (Fe-0.9Cu-1.0).

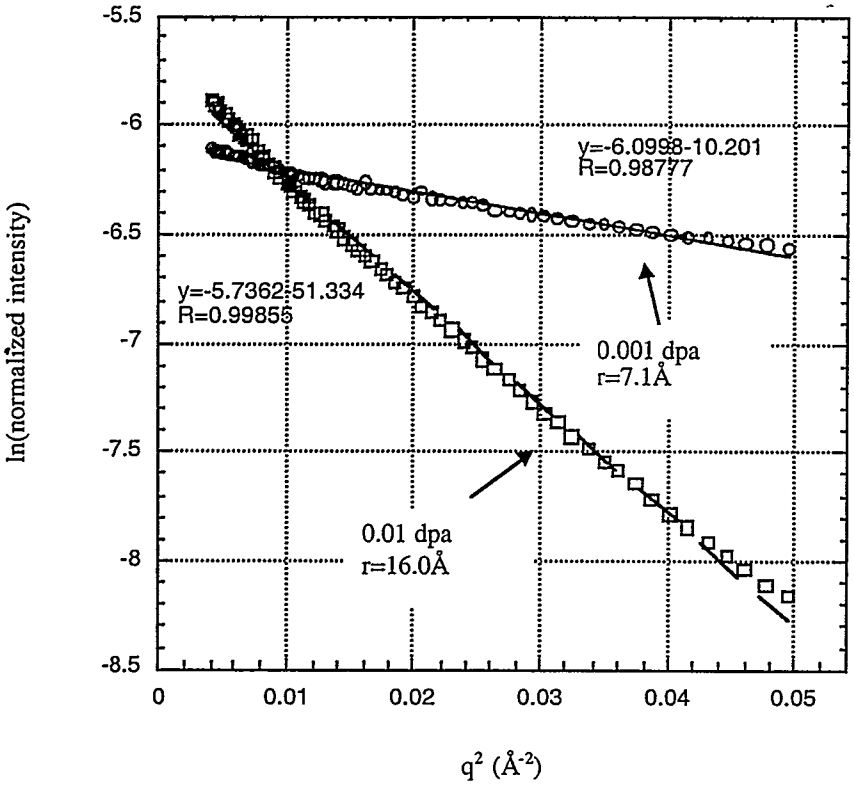

Figure 9. The relation of ln$I$ and q^2 for the VD alloy irradiated with protons to doses of 0.001 and 0.01 dpa at 300°C and a dose rate of $7x10^{-7}$dpa/s.

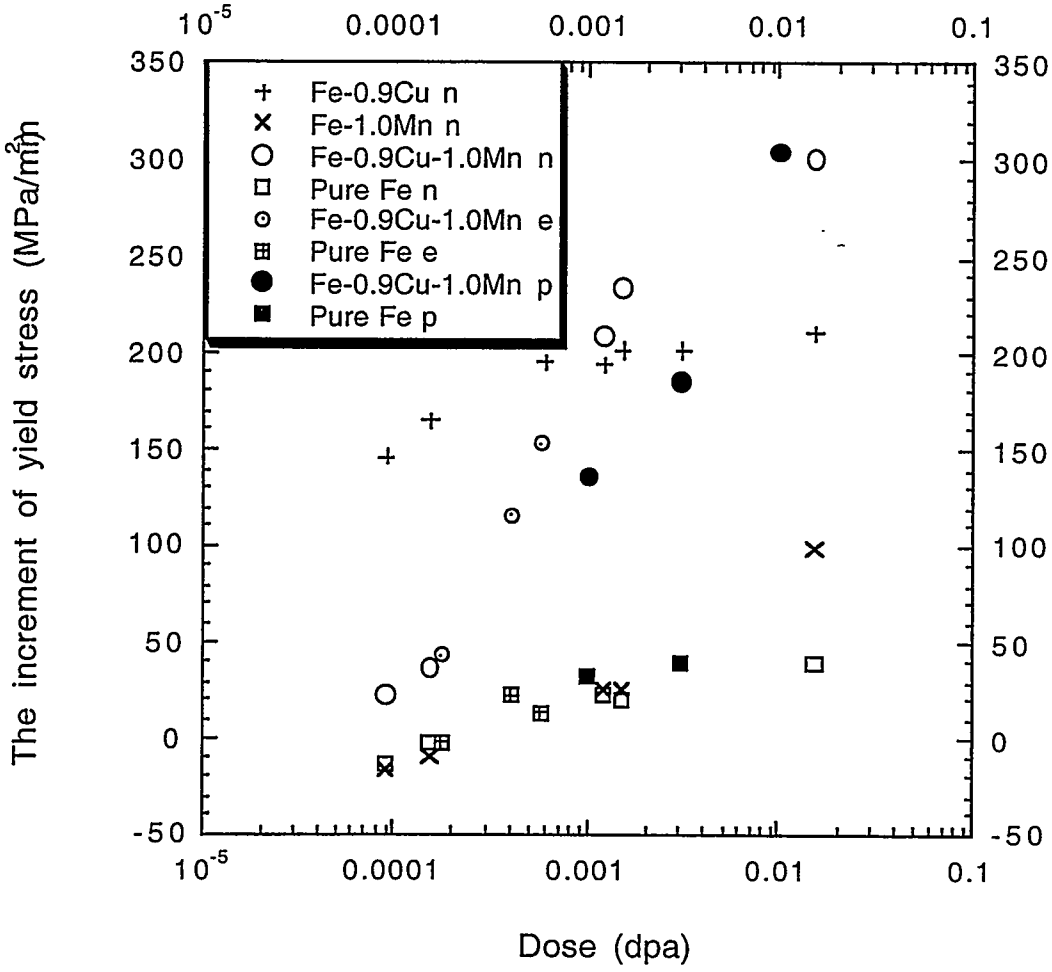

Figure 10. Yield strength increase as a function of dose for several alloys and several irradiating particles (n=neutron, p=proton, e=electron).